nuclear fusion
IAEA

PAPER • OPEN ACCESS

Synergistic effect between radial electric field and magnetic shear on ion temperature gradient mode

To cite this article: Qien Jing *et al* 2025 *Nucl. Fusion* **65** 106037

OPEN ACCESS
IOP Publishing | International Atomic Energy Agency
Nuclear Fusion
Nucl. Fusion **65** (2025) 106037 (10pp)
https://doi.org/10.1088/1741-4326/ae074f

Synergistic effect between radial electric field and magnetic shear on ion temperature gradient mode

Qien Jing[1], Yuehao Ma[1,*], Huishan Cai[1,*] and Zhihong Lin[2]

[1] CAS Key Laboratory of Frontier in Controlled Nuclear Fusion, and School of Nuclear Sciences and Technology, University of Science and Technology Technology of China, Hefei 230031, China
[2] Department of Physics and Astronomy, University of California, Irvine, CA 92697, United States of America

E-mail: myh2020@mail.ustc.edu.cn and hscai@mail.ustc.edu.cn

Received 6 January 2025, revised 13 September 2025
Accepted for publication 16 September 2025
Published 25 September 2025

Abstract

The synergistic effect between the radial electric field (E_r) shear and the magnetic shear on the ion temperature gradient (ITG) mode in a Experimental Advanced Superconducting Tokamak discharge has been investigated using gyrokinetic simulations. The stabilizing or destabilizing effect of the E_r shear depends on both its magnitude and its directional alignment with the magnetic shear, with a negative shearing rate exhibiting a more efficient stabilizing influence under the weakly reversed magnetic shear because both effects tilt the ITG mode structure in the same direction. Nonlinear simulations reveal a threshold in shearing rate beyond which the E_r shear suppresses the ITG turbulence and highlight the enhanced suppression of the ITG turbulence by the negative shearing rate under the weakly reversed magnetic shear. Based on the experimental E_r profile, it is shown that the geometric effect of E_r on the stabilization of micro-instabilities needs to be considered. The relative position between the bottom of the well-like experimental E_r and the ITG mode is crucial for effectively stabilizing the ITG mode, highlighting the synergistic effect between the E_r shear and the magnetic shear on the ITG mode.

Keywords: radial electric field, ion temperature gradient mode, magnetic shear

(Some figures may appear in colour only in the online journal)

* Authors to whom any correspondence should be addressed.

1. Introduction

Turbulent transport driven by drift-wave instabilities has been widely observed in fusion plasmas, significantly degrading the confinement performance of tokamaks [1, 2]. Among these instabilities, the ion temperature gradient (ITG) mode is particularly crucial, as it predominantly governs ion heat transport, and its suppression is essential for the formation of transport barriers [1–12]. The radial electric field shear (E_r shear), quantified by the shearing rate (ω_s), is known to stabilize the ITG turbulence and promotes the formation of internal transport barrier (ITB) [12–17]. On the other hand, experimental observations suggest that the formation of ITB is facilitated under conditions of weakly reversed magnetic shear [3, 6, 8–11]. Therefore, the E_r shear and the magnetic shear may play a significant role in suppressing the ITG turbulence and promoting the formation of ITB.

It is well-known that radial electric field (E_r) shear can suppress turbulence either by tilting the mode structure or by breaking up turbulent eddies [14, 17–20]. Global linear gyrokinetic simulations have shown an asymmetric stabilization behavior by flow shear, arising from the competition between equilibrium profile variations and E_r shear [20, 21]. Previous studies based on the cyclone base case (CBC) configuration with normal magnetic shear have also demonstrated that the increasing magnetic shear enhances the stabilizing effects of E_r shear on the linear growth rate of the ITG instability [14]. Furthermore, global linear simulations indicate that the symmetry-breaking effect of E_r shear on the parallel wave number becomes more pronounced in weakly normal magnetic shear configurations [10]. However, research focusing on synergistic effects between the E_r shear and the reversed magnetic shear, especially in the nonlinear regime, remains limited and warrants further investigation.

In this work, we investigate the synergistic effect between the E_r shear and the magnetic shear on the ITG turbulence in Experimental Advanced Superconducting Tokamak (EAST) discharge #93890 [22]. Linear simulation results indicate an asymmetry in the suppression of the ITG turbulence with respect to the sign of the E_r shearing rate, due to competition between the magnetic shear and the E_r shear. Nonlinear simulations further demonstrate the importance of the synergistic effect in nonlinear stage, showing that a E_r shear with negative shearing rate under weakly reversed magnetic shear can more effectively suppress the ITG turbulence amplitude and the turbulent transport. Moreover, in the presence of weakly reversed magnetic shear, effective suppression of the ITG turbulence is achieved only when ω_s exceeds a certain threshold.

The remainder of this paper is organized as follows. The physical model and simulation setup are described in section 2. The synergistic effect between the E_r shear and the magnetic shear on the ITG mode in linear growth stage and nonlinear stage of the ITG turbulence is discussed in section 3. The simulation with experimental E_r on EAST is discussed in section 4.

2. Physical model and simulation setup

This study focuses on the synergistic effect between the equilibrium radial electric fields shear and the magnetic shear on electrostatic drift wave turbulence. The detail of the gyrokinetic models utilized in the GTC code have been previously discussed in [13, 23, 24]. To account for the influence of the equilibrium radial electric field E_r, the electrostatic potential $\phi = \delta\phi + \phi_{eq}$ is incorporated into the gyrokinetic equations [13], where $\delta\phi$ is the perturbed electrostatic potential and ϕ_{eq} is the equilibrium electrostatic potential [17]. The equilibrium electric field will impact the ITG mode in two important ways. Firstly, the rigid rotation caused by $E \times B$ drift will change the frequency of the ITG mode, i.e. Doppler shift $\Omega_E = -n\mathrm{d}\phi_{eq}/\mathrm{d}\psi$ [18]. Secondly, the sheared flow caused by E_r will stabilize the ITG mode and affect the saturation amplitude, while the shearing rate: $\omega_s = -\frac{(R_0 B_p)^2}{B_0}\partial^2\phi_{eq}/\partial\psi^2$ is used for describing the E_r shear effect [25].

In our study, the simulations of electrostatic turbulence are conducted using experimental data from EAST tokamak discharge (#93890) at 5000 ms, where both the plasma profile and magnetic geometry have previously been discussed in [22, 24]. As shown in figure 1, both the electron and ion densities, as well as temperatures, exhibit an ITB in the presence of weakly negative magnetic shear. The detailed parameters are as follows. The on-axis major radius is $R_0 = 1.91$ m, the minor radius at the wall of the outer mid-plane is $a = 0.41$ m, and the on-axis magnetic field of is $B_0 = 1.49$ T, while the maximum value of $\eta_i = L_{ni}/L_{Ti}$ is located at $r/a \approx 0.25$ [24], providing the toroidal ITG drive. Our simulation domain is delineated in the radial normalized range $r/a \in [0.10, 0.52]$. Dirichlet boundary conditions are applied due to the negligible turbulence perturbations near the boundary. The other simulation parameters used for convergent physical run are 150 radial grids, 32 toroidal grids and 600 poloidal grids in the simulation domain. The time step is $\Delta t = 0.005 R_0/C_s$ (where C_s is the sound speed on magnetic axis).

3. Synergistic effect between the E_r shear and the magnetic shear

3.1. ITG mode dispersion relation and frequency Doppler shift caused by E_r

To study the synergistic effect between the E_r shear and the magnetic shear on stabilizing the ITG mode, the dispersion relation with E_r shear should be verified in the physical model. The dispersion relation without E_r shear in the simulation domain has been well researched previously in the report [24], showing that the most unstable mode corresponding to $k_\theta \rho_i \approx 0.9$ ($n = 25$), where the $\rho_i = 0.0037$ m is the ion gyroradius. Now, we use a constant $\mathrm{d}\phi/\mathrm{d}\psi$ ($\omega_s = 0$) profile to verify the Doppler shift effect on the ITG mode. The simulation results of the mode frequency, both without E_r and with E_r ($\omega_s = 0$), are depicted in figure 2(*a*). The simulation results with E_r

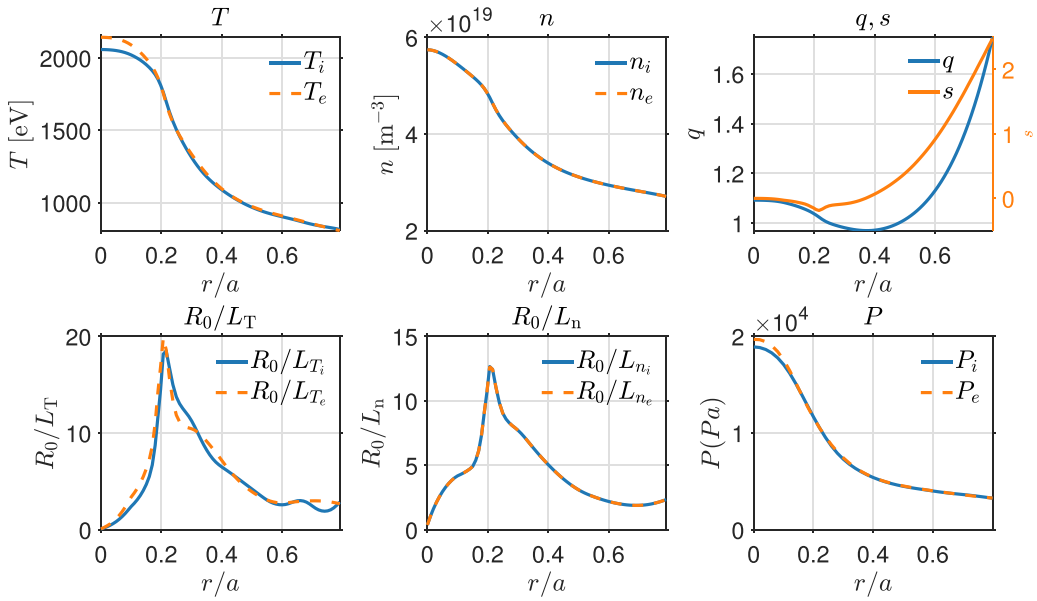

Figure 1. Plasma radial profile in EAST discharge #93890 at 5000 ms. The top row, from left to right, shows temperatures (T), density (n) for ions (subscript i) and electrons (subscript e), safety factor (q) and magnetic shear (s) respectively. The bottom row, from left to right, shows the inverse temperature length scales (R_0/L_T), the inverse density length scale (R_0/L_n), pressure for ions and electrons respectively.

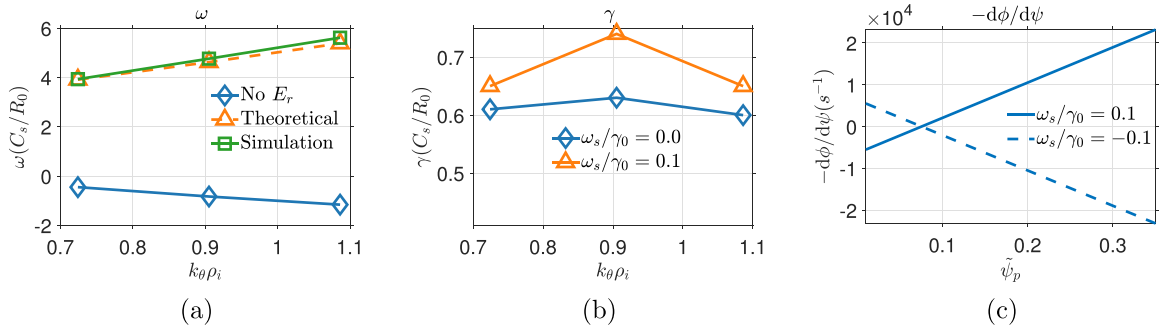

Figure 2. (a) Mode frequencies of the ITG mode are shown as the blue line (without E_r), the green line (E_r with $\omega_s = 0$), and the orange dashed line (theoretical results calculated by the theory in [18]). (b) Linear growth rate of the ITG mode as a function of poloidal wavelength $k_\theta\rho_i$ (corresponding to toroidal mode numbers $n = 20,\ 25,\ 30$) under constant normalized E_r shearing rates ω_s/γ_0, where γ_0 is the linear growth rate without E_r shear. The E_r profiles corresponding to constant $\omega_s/\gamma_0 = \pm 0.1$ are shown in figure (c). (c) The E_r with $\omega_s/\gamma_0 = \pm 0.1$ represented by $\mathrm{d}\phi/\mathrm{d}\psi$ over normalized poloidal flux and the E_r with different ω_s/γ_0 is generated by changing the slope of the $\mathrm{d}\phi/\mathrm{d}\psi$.

($\omega_s = 0$) agree well with the theoretical results calculated by the Doppler shifted effect [18]. Additionally, the linear growth rates without E_r and with E_r ($\omega_s = 0$) have no obvious difference, indicating the E_r with $\omega_s = 0$ has nearly no stabilizing effect on the ITG mode.

Moreover, to verify the impact of the E_r shear on the linear growth rate of the ITG modes, the dependence of linear growth rate on poloidal wavelength $k_\theta\rho_i$ under E_r with constant $\omega_s/\gamma_0 = 0, 0.1$ is shown in figure 2(b), where γ_0 denotes the linear growth rate of the ITG mode at $k_\theta\rho_i \approx 0.9$ (corresponding to the most unstable toroidal mode number $n = 25$) in the absence of E_r. However, the presence of E_r shear increases the linear growth rate, which is opposite to the result where E_r shear decreases the linear growth rate of the ITG mode [13–15]. Next, we focus on the most unstable case ($n = 25$) to study the synergistic effect between the E_r shear and the magnetic shear on the ITG mode.

3.2. Synergistic effect between the E_r shear and the magnetic shear on the linear growth of ITG

The synergistic effect between the E_r shear and the magnetic shear in the linear growth stage is further explored in this section. First, it is necessary to understand the impact of the magnetic shear on the ITG mode in the linear growth stage in the absence of the E_r shear. By using different q profiles, we obtain various magnetic shear values at the ITG mode location (specifically, $s = -0.13,\ 0.2,\ 0.4,\ 0.6,\ 0.8$), and compare the stabilizing effects of E_r shear under these different magnetic shear, where the original weakly reversed magnetic shear is $s = -0.13$. The selected q profiles are shown in figure 3(a). As illustrated in figure 4(a), the ITG mode is gradually destabilized with increasing magnetic shear in the range $s = [-0.13,\ 0.8]$ in the absence of the E_r shear. This trend arises from the progressive anticlockwise tilting

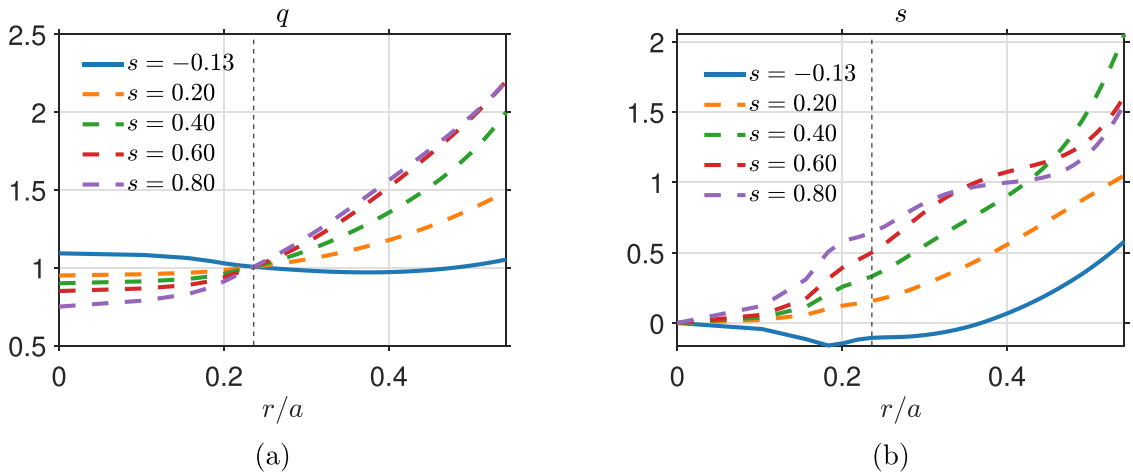

Figure 3. (*a*) The safety factor q profiles used to generate different magnetic shear values. (*b*) Corresponding magnetic shear (s) profiles. Note that the values of s shown in the legend correspond to their values at the ITG mode location, indicated by the gray dashed line.

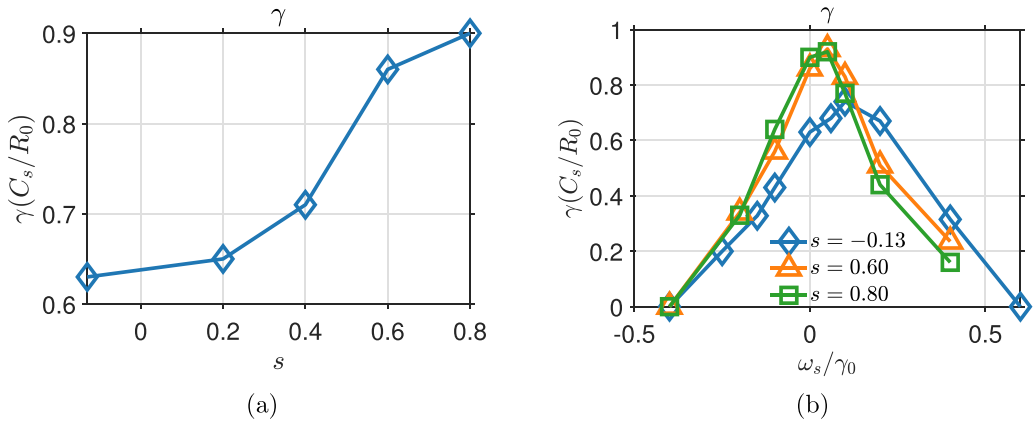

Figure 4. (*a*) ITG linear growth rate γ as a function of magnetic shear s in the absence of E_r. (*b*) ITG linear growth rate γ versus ω_s/γ_0, for three cases with $s = -0.13, 0.6, 0.8$, as shown in figure 3(*b*). For each value of s, the normalization factor γ_0 corresponds to the ITG linear growth rate without E_r shear at that specific magnetic shear.

of the ITG mode structure as the magnetic shear decreasing, with the increasing tilt effect leading to a lower linear growth rate [4, 26], as illustrated in figures 5(*a*)–(*c*). Moreover, as the magnetic shear increase, the coupling between different poloidal (m) harmonics becomes weaker, which contributes to the destabilization of the ITG mode, as shown in figures 5(*d*)–(*f*).

Second, building on the understanding of the tilting effect of magnetic shear on the ITG mode, we further investigate the synergistic effect between the E_r shear and the magnetic shear. The ITG linear growth rate γ as a function of normalized shearing rate ω_s/γ_0 for different magnetic shear values are shown in figure 4(*b*). It is important to note that, for each magnetic shear s, the normalization factor γ_0 refers to the linear growth rate at that respective s in the absence of E_r shear. Under original weakly reversed magnetic shear ($s = -0.13$), the ITG mode becomes destabilized with increasing positive ω_s, reaching a maximum growth rate at $\omega_s/\gamma_0 = 0.1$. Beyond this point, further increase in positive ω_s leads to stabilization. In contrast, for negative ω_s, the ITG mode is monotonically stabilized as $|\omega_s|$ increases. These results indicate the non-symmetric dependence (i.e. ω_s sign-dependent) of the linear growth rate of a global ITG mode as a function of the shearing rate under weakly reversed magnetic shear. This behavior differs from that observed in previous CBC studies [13–15], where the stabilizing effect appeared to be ω_s sign-independent. The following provides a physical explanation for the results presented above. The two-dimensional poloidal cross-sections of the perturbed electrostatic potential $\delta\phi$ with different constant ω_s/γ_0 are shown in figure 6, corresponding to the results of the blue curve in figure 4(*b*). As illustrated in figure 6(*b*), in absence of the E_r shear ($\omega_s = 0$), the ITG mode structure, though centered near the midplane, is tilted in the anticlockwise direction by the magnetic shear. When E_r shear is introduced, the mode is tilted further: positive ω_s induces a clockwise tilt, while negative ω_s enhances the anticlockwise tilt. Consequently, they either counteract or reinforce the tilt induced by the magnetic shear, resulting

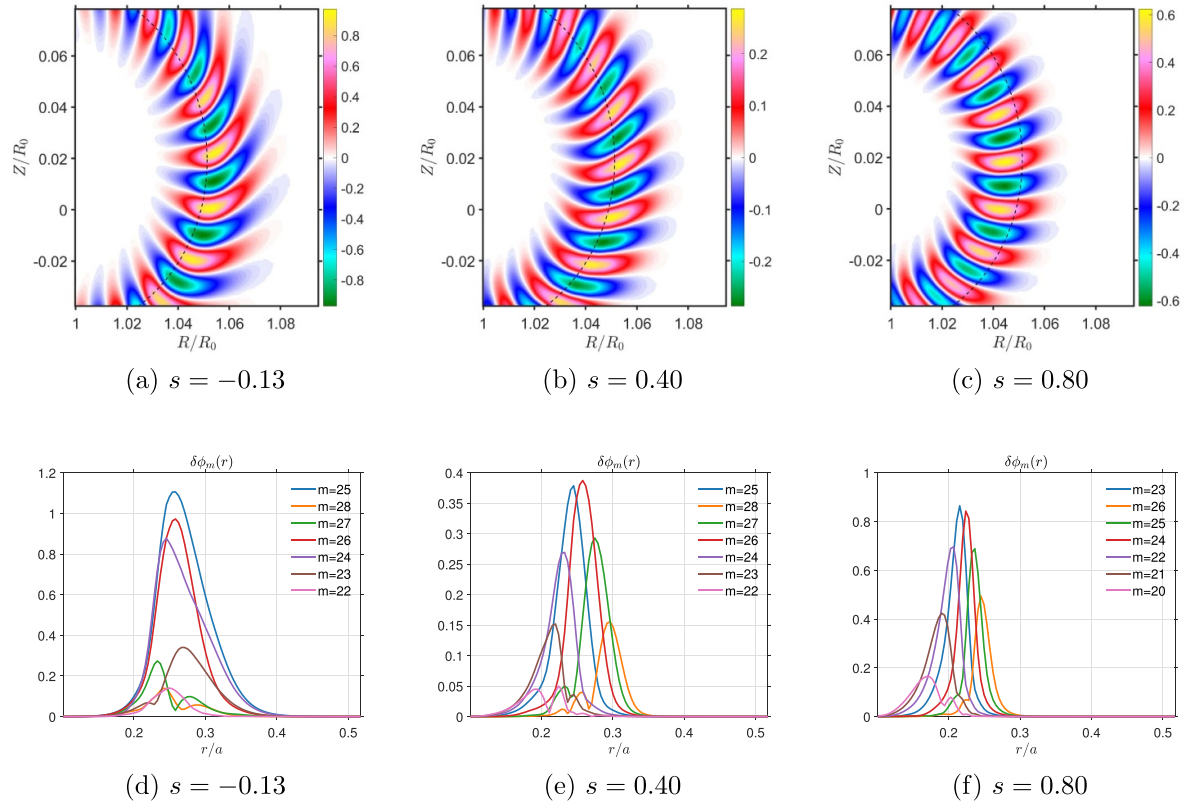

(a) $s = -0.13$ (b) $s = 0.40$ (c) $s = 0.80$

(d) $s = -0.13$ (e) $s = 0.40$ (f) $s = 0.80$

Figure 5. (*a*)–(*c*) Show the two-dimensional poloidal contour of perturbed electrostatic potential $\delta\phi$ with magnetic shear $s = -0.13, 0.40, 0.80$ shown in figure 3(*b*), respectively. (*d*)–(*f*) Show the radial mode profile of different poloidal mode numbers m corresponding the mode structures in top panels.

in an destabilizing or stabilizing effect on the ITG mode, respectively.

Under stronger magnetic shear ($s = 0.6,\ 0.8$), the shearing rate corresponding to the maximum linear growth rate shifts to $\omega_s/\gamma_0 \approx 0.05$, which is lower than that under weakly reversed magnetic shear, where $\omega_s/\gamma_0 \approx 0.10$. This shift occurs because the weak tilting effect induced by stronger magnetic shear, as seen in figures 5(*b*) and (*c*), allowing the E_r shear to dominate the mode tilting. Moreover, the stabilization of the ITG mode by negative ω_s is less effective under stronger positive magnetic shear than under weakly reversed magnetic shear, underscoring the synergistic effect between the negative ω_s and the weakly reversed magnetic shear in achieving efficient stabilization. These results highlight the importance of simultaneously optimizing magnetic shear and E_r shear in order to maximize the stabilizing effect on the ITG modes.

3.3. Synergistic effect between the E_r shear and the magnetic shear in the nonlinear stage

In this section, nonlinear simulations are conducted to investigate the synergistic effect between the E_r shear and the magnetic shear on the ITG turbulence. The time evolution of the ITG turbulence amplitude $\delta\phi$ for modes $n = 0,\ 15,\ 20,\ 25,\ 30$ in the absence of E_r shear is shown in figure 7(*a*). As time increases, the amplitude of $\delta\phi$ exhibits exponential growth and enters the nonlinear saturation stage after $t = 25\ R_0/C_s$. The two-dimensional poloidal contour of $\delta\phi$ at the nonlinear saturation time $t = 26\ C_s/R_0$ without E_r is shown in figure 7(*b*).

To investigate the impact of the E_r shear during the nonlinear stage, it is applied at $t = 15\,C_s/R_0$, during the linear phase before ITG turbulence saturation. To estimate the radial correlation length of the turbulence, we calculate the two-point correlation function [18]:

$$C_r(\Delta r, \Delta\theta) = \frac{\langle \delta\phi\,(r+\Delta r, \theta+\Delta\theta)\,\delta\phi\,(r,\theta)\rangle}{\sqrt{\langle \delta\phi^2\,(r+\Delta r, \theta+\Delta\theta)\rangle\,\langle \delta\phi^2\,(r,\theta)\rangle}} \qquad (1)$$

where Δr and $\Delta\theta$ represent the radial and poloidal separations, respectively, and $\langle\ \rangle$ represents the average over the radial and poloidal space. To obtain the one-dimensional radial correlation function $C_r(\Delta r)$, we extract the maximum value along the ridge of $C_r(\Delta r, \Delta\theta)$. At small radial separations, the 1D radial correlation function decays in a Gaussian manner: $C_r(\Delta r) \approx \exp\left[-(\Delta r/L_r)^2\right]$, with L_r representing the turbulence correlation length in the radial direction.

The turbulence amplitude $\delta\phi$ and correlation length of the turbulence L_r as a function of the normalized shearing rate ω_s/γ_0 for magnetic shear values of $s = -0.13$ and $s = 0.80$ are shown in figure 8. The $\delta\phi$ are obtained by time-averaged over the nonlinear saturation stage. As shown in figure 8(*a*), the E_r shear with low ω_s fails to effectively suppress the

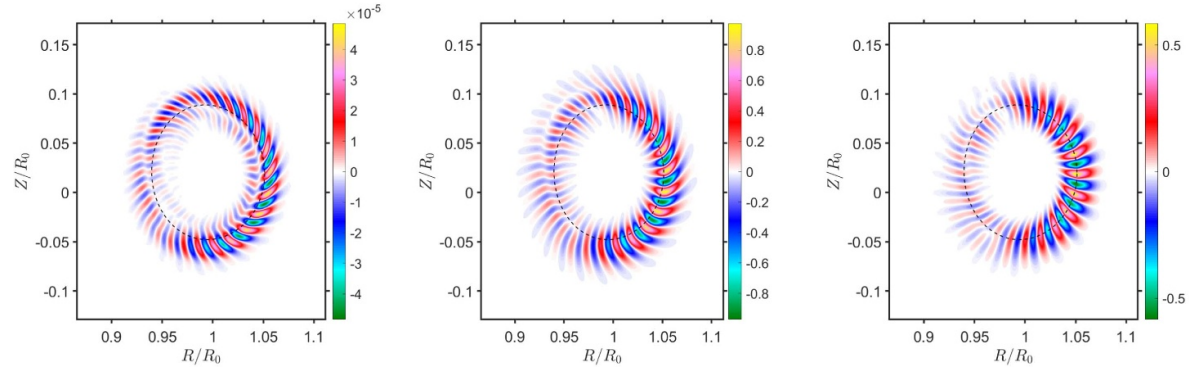

Figure 6. The two-dimensional poloidal contour of perturbed electrostatic potential $\delta\phi$ with constant $\omega_s/\gamma_0 = -0.1, 0.0, 0.1$. The dashed line indicates the largest η_i and $q = 1$ positions.

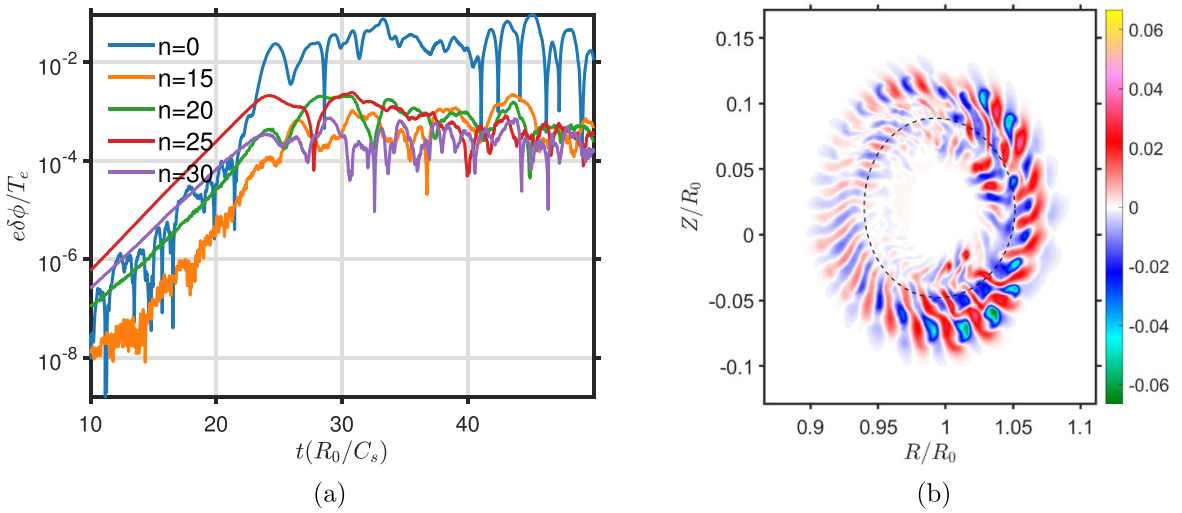

Figure 7. (*a*) Time evolution of the ITG turbulence amplitude $\delta\phi$ for modes with $n = 0,\ 15,\ 20,\ 25,\ 30$ in the absence of E_r shear. (*b*) Two-dimensional poloidal contour of the perturbed electrostatic potential $\delta\phi$ at the nonlinear saturation time $t = 26\ C_s/R_0$, also without E_r shear.

amplitude of the ITG turbulence under $s = -0.13$, forming a plateau structure within the range of $\omega_s/\gamma_0 = [-0.1, 0.3]$. However, as $|\omega_s|$ increases, the E_r shear becomes increasingly effective in reducing the amplitude of the ITG turbulence. Additional, the ITG turbulence amplitude is more effectively suppressed by E_r shear with negative ω_s compared to positive ω_s, as demonstrated by the results at $\omega_s = \pm 0.4, \pm 0.6$. For $s = 0.80$, as shown in figure 8(*b*), $\delta\phi$ increases slightly as ω_s/γ_0 rises from 0 to $+0.1$, and then decreases with further increasing $|\omega_s|$. In contrast, for negative ω_s, $\delta\phi$ decreases monotonically with increasing $|\omega_s|$, without exhibiting a plateau structure as observed in the case under weakly reversed magnetic shear. Moreover, the difference in the suppression effect between the positive and the negative ω_s is less pronounced compared to the case under weakly reversed magnetic shear. The dependence of L_r on ω_s exhibits a trend similar to that of $\delta\phi$ for both magnetic shear conditions, although the reduction in $\delta\phi$ is more pronounced than that in L_r. Furthermore, the dependence of both quantities on ω_s is asymmetric, which is consistent with the asymmetric response of the linear growth rate to ω_s observed in linear simulations.

The ion heat diffusivity χ_i, obtained by time-averaged over the nonlinear saturation stage, as a function of the normalized shearing rate ω_s/γ_0 for magnetic shear values of $s = -0.13$ and $s = 0.80$ are shown in figure 9. For both magnetic shear conditions, the variation of χ_i with respect to ω_s/γ_0 closely resembles that of $\delta\phi$. Under $s = -0.13$, the E_r shear within the range $\omega_s/\gamma_0 = [-0.1,\ 0.3]$ has little effect on χ_i. However, as $|\omega_s|$ increases further, χ_i decreases significantly. Similarly, E_r shear with negative ω_s suppresses χ_i more effectively than with positive ω_s, as seen at $\omega_s = \pm 0.4,\ \pm 0.6$. Under $s = 0.80$, χ_i slightly increases from $\omega_s/\gamma_0 = 0$ to $+0.1$, then decreases as $|\omega_s|$ increases, without the plateau observed in the $s = -0.13$ case. In contrast, χ_i decreases monotonically for negative ω_s. Moreover, the difference in the suppression effect between the

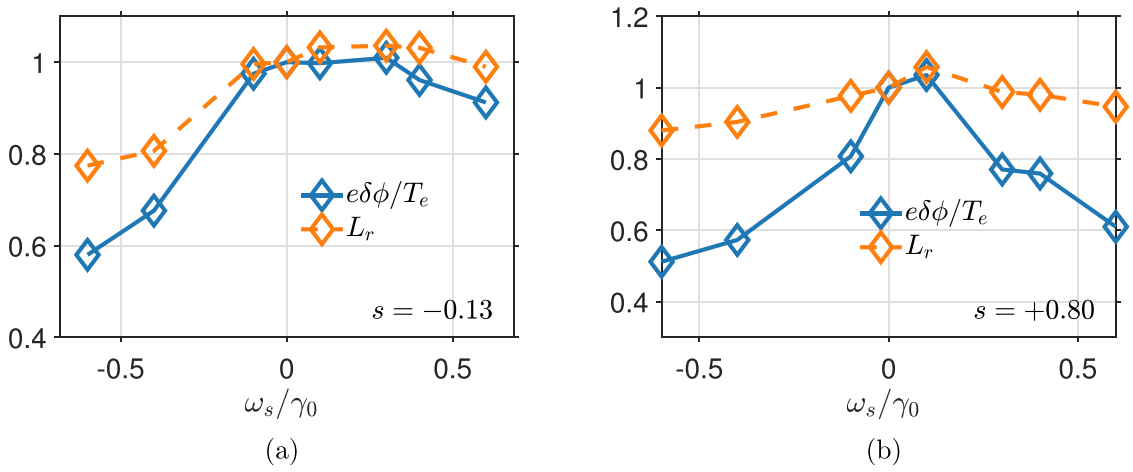

Figure 8. (*a*) and (*b*) Show the nonlinear ITG turbulence amplitude $\delta\phi$ and the radial correlation length L_r, respectively, as functions of the normalized E_r shearing rate ω_s/γ_0, for magnetic shear values of $s = -0.13$ and $+0.80$. Both quantities are normalized by their values for the case of $\omega_s/\gamma_0 = 0$.

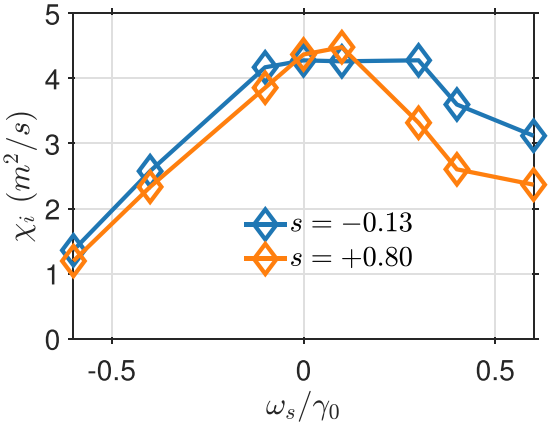

Figure 9. The nonlinear heat diffusivity of ions χ_i as a function of the normalized E_r shearing rate ω_s/γ_0 for magnetic shear $s = -0.13,\ +0.80$, respectively.

positive and the negative ω_s is less pronounced compared to the case under $s = -0.13$.

In summary, nonlinear simulation results highlight the existence of a threshold in ω_s, beyond which the E_r shear effectively suppresses the ITG turbulence amplitude and ion heat diffusivity under weakly reversed magnetic shear. The results further demonstrate a clear synergistic effect between the E_r shear and the magnetic shear in nonlinear stage, consistent with trends observed in linear stage. Notably, negative ω_s under weakly negative magnetic shear yields more pronounced suppression than positive ω_s, while this asymmetry becomes less significant under positive magnetic shear ($s = +0.80$).

4. Geometric effect of experimental E_r on the ITG turbulence

Building on the previous finding that, under weakly reversed magnetic shear, the E_r shear with a negative shearing rate suppresses the ITG turbulence more effectively than a positive one, it becomes crucial to consider experimental radial electric fields in order to achieve efficient the ITG turbulence suppression and facilitate the formation of ITBs. We use the parameters based on a ITB formed case at 5000 ms on EAST [22] to calculated experimental E_r profile from the radial force balance equation:

$$\partial\phi_{\rm eq}/\partial\psi = -\frac{1}{n_i Z_i}\partial P_i/\partial\psi + q\Omega_\theta - \Omega_\phi \qquad (2)$$

where n_i and P_i are the ion density and pressure, q is the safety factor, Ω_θ is the poloidal rotation, ψ is the poloidal flux. In this work, we focus on the discharges with weak external torque, where the ion pressure gradient dominates the radial force balance and the effects of rotational terms can be neglected [22]. The blue curve in figure 10(*a*) shows the experimentally derived E_r profile, which exhibits a well-like shape, with its minimum (corresponding to $\omega_s = 0$) located at $r/a = 0.20$. Linear simulations based on this E_r profile indicate that the ITG mode is completely stabilized. To further understand the behavior of the ITG modes under the experimental E_r profile, we analyze both the amplitude of E_r and the $\omega_s = 0$ location of the E_r. Given the small radial extent of the ITG mode structure, it is possible that the mode experiences no shear at the point where $\omega_s = 0$.

First, we vary the amplitude of the experimental E_r profile by multiplying it with a scaling factor, while keeping the location of its bottom at $r/a = 0.20$. The linear simulation results are shown by the orange curve in figure 10(*b*), where $\omega_s^{\max}$ the maximum shearing rate (ω_s) across the radial domain, is used to quantify the amplitude of the E_r profile. The orange curve suggests that the experimental well-like E_r profile stabilizes the ITG mode more effectively than the E_r profile with constant ω_s (blue curve) in the low ω_s regime.

Secondly, we investigate the effect of varying the radial location where $\omega_s = 0$. The ITG linear growth rate as a function of $\omega_s^{\max}/\gamma_0$ for experimental E_r profiles with $\omega_s = 0$ located at $r/a = 0.20,\ 0.25,\ 0.30$ are shown in figure 10(*b*). These

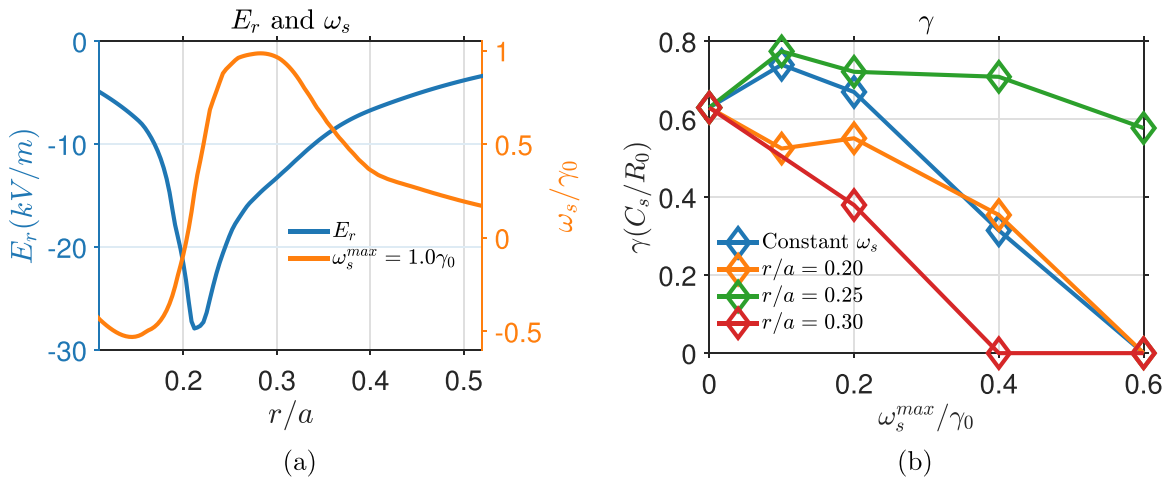

Figure 10. (*a*) The experimental E_r directly calculated by the radial force balance equation and the corresponding shearing rate are represented by blue and yellow curve, respectively. (*b*) The orange, green, and red curves show the ITG linear growth rate as a function of $\omega_s^{\max}$ for experimental E_r profiles with $\omega_s = 0$ at $r/a = 0.20,\ 0.25,\ 0.30$, respectively. The blue curve represents the case with a constant ω_s E_r profile, identical to the blue curve in figure 4(*b*). Note that for a constant ω_s profile, ω_s is uniform across the radial domain, i.e. $\omega_s = \omega_s^{\max}$ everywhere.

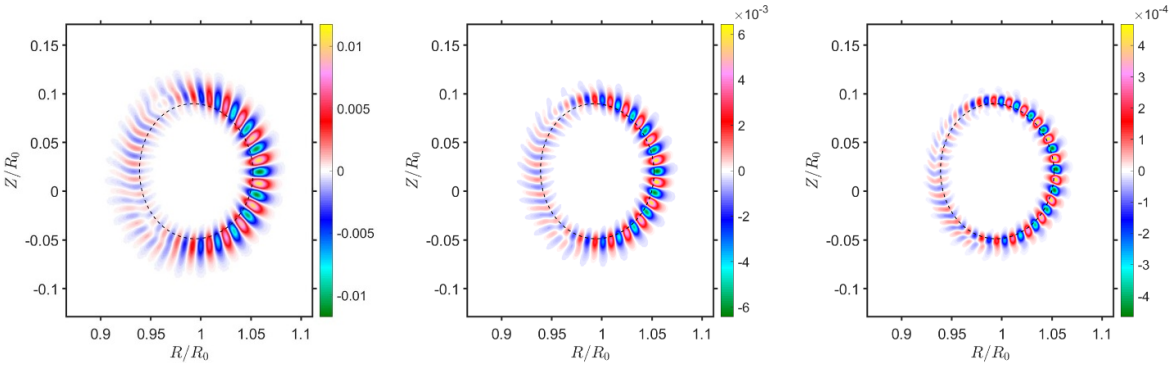

Figure 11. The two-dimensional poloidal contour of perturbed electrostatic potential $\delta\phi$ with experimental E_r which $\omega_s = 0$ at $r/a = 0.25$. The $\omega_s^{\max}/\gamma_0 = 0.2, 0.4, 1.0$, respectively, and the dashed line indicates the $q = 1$ surface.

three profiles are obtained by shifting the original E_r profile along the radial direction. The shifted positions ($r/a = 0.20,\ 0.25,\ 0.30$) correspond to the inner side, center, and outer side of the ITG mode region, respectively. When $\omega_s = 0$ is located at $r/a = 0.30$, where the ITG mode experiences negative ω_s, the linear growth rate decreases rapidly with increasing $\omega_s^{\max}/\gamma_0$, indicating stronger suppression than in other E_r profiles. This observation is consistent with the mechanism discussed earlier, in which negative ω_s shear is more effective than positive shear in stabilizing ITG modes under weakly reversed magnetic shear. In contrast, when $\omega_s = 0$ is positioned at $r/a = 0.25$, the linear growth rate shows little reduction, indicating that the E_r shear has a negligible stabilizing effect in this case. This result can be explained by the physical interpretation provided in section 3. As the amplitude of the E_r profile increases, the surrounding ω_s increases accordingly, which shortens the ITG mode wavelength [17], while the $\omega_s = 0$ remains located at the mode location. Consequently, the mode structure experiences minimal tilting, and no significant reduction in the linear growth rate is observed, as shown in figures 11(*a*)–(*c*). These results suggest that the local minimum of the E_r well ($\omega_s = 0$ region) is the least favorable region for the suppression of the ITG mode.

Simulation results based on the experimental E_r profile suggest that the geometric effect of E_r must be considered. In particular, the bottom of the E_r well is the least favorable location for the stabilization of the ITG mode by the E_r shear. In the experiment, the formation of the ITB in the plasma core is accompanied by increases in ion temperature and density [1, 2, 11], which steepen the ion pressure gradient and consequently enhance the amplitude of E_r. Furthermore, the experiment observation [27] showed an outward radial shift of the E_r well, consistent with our finding that an $\omega_s = 0$ profile positioned farther out more effectively stabilizes the ITG mode. This enhanced stabilization arises from the synergistic effect between the negative ω_s and the weakly reversed magnetic shear. These observations may suggest the presence of a positive feedback mechanism between the ITB formation

and the evolution of the E_r profile. As ITG turbulence is suppressed, the resulting enhancement in the ion pressure gradient leads to an increase in the E_r amplitude and an outward shift of the $\omega_s = 0$ point; together with reversed magnetic shear, this can further suppress the ITG turbulence. Such a positive feedback loop may play a critical role in the formation of the ITB in the plasma core. To further suppress ITG-driven transport, it is beneficial to shape the E_r structure so that negative ω_s is aligned with the reversed magnetic shear region. This could be realized, for instance, by applying neutral beam injection to induce plasma rotation and thereby modify the E_r profile [28].

5. Conclusion

Based on EAST configuration, the synergistic effect between the E_r shear and the magnetic shear on the ITG turbulence is studied by GTC.

Linear simulation results indicate an asymmetry in the suppression of the ITG turbulence with respect to the sign of the E_r shearing rate, due to competition between the magnetic shear and the E_r shear. Under the weakly reversed magnetic shear, E_r shear is destabilizing for small positive shearing rate, while it is stabilizing when positive shearing rate is large enough. For negative shearing rate, E_r shear always plays a stable role, and is more efficient than that with positive shearing rate. Because the negative ω_s shear and the weakly magnetic shear have the same mode tilting direction. The simulation results indicate that the ITG mode is more unstable under the positive magnetic shear. Nonlinear simulations further demonstrate the importance of the synergistic effect in nonlinear stage, showing that a E_r shear with negative shearing rate under weakly reversed magnetic shear can more effectively suppress the ITG turbulence amplitude and the turbulent transport. Moreover, in the presence of weakly reversed magnetic shear, effective suppression of the ITG turbulence is achieved only when ω_s exceeds a certain threshold. The experimental E_r profile simulations indicates that the geometric effect of E_r profile should be considered in stabilizing the ITG instability for experimental E_r. The well-like E_r profile with $\omega_s = 0$ located outside the ITG mode stabilizes it more effectively than when $\omega_s = 0$ is located inside, due to the synergistic effect between the negative ω_s shear and the weakly reversed magnetic shear. The positive feedback loop between the formation of ITB and the E_r profile that amplifies the E_r amplitude and shifts its bottom outward, which might be the key to the formation of ITB.

Acknowledgments

This work is supported by the National Key R&D Program of China (Grant No. 2024YFE03050002), National Natural Science Foundation of China (Grant No. 12525511 and No. 12025508), and the Strategic Priority Research Program of Chinese Academy of Sciences (Grant Nos. XDB0500302 and XDB0790202). The numerical calculations in this paper were performed on the Hefei Advanced Computing Center.

ORCID iDs

Qien Jing 0009-0003-1241-6943
Yuehao Ma 0009-0007-8034-5402
Huishan Cai 0000-0002-2500-3721
Zhihong Lin 0000-0003-2007-8983

References

[1] Wagner F. *et al* 1982 Regime of improved confinement and high beta in neutral-beam-heated divertor discharges of the asdex tokamak *Phys. Rev. Lett.* **49** 1408–12
[2] Wagner F. 2007 A quarter-century of h-mode studies *Plasma Phys. Control. Fusion* **49** B1
[3] Koide Y. *et al* 1994 Internal transport barrier on q = 3 surface and poloidal plasma spin up in Jt-60U high-β_p discharges *Phys. Rev. Lett.* **72** 3662–5
[4] Antonsen Jr. T.M., Drake J.F., Guzdar P.N., Hassam A.B., Lau Y.T., Liu C.S. and Novakovskii. S.V. 1996 Physical mechanism of enhanced stability from negative shear in tokamaks: implications for edge transport and the L-H transition *Phys. Plasmas* **3** 2221–3
[5] Burrell K.H., Austin M.E., Greenfield C.M., Lao L.L., Rice B.W., Staebler G.M. and Stallard B.W. 1998 Effects of velocity shear and magnetic shear in the formation of core transport barriers in the DIII-D tokamak *Plasma Phys. Control. Fusion* **40** 1585
[6] Connor J.W., Fukuda T., Garbet X., Gormezano C., Mukhovatov V. and Wakatani M. (the ITB Database Group, the ITPA Topical Group on Transport and Internal Barrier Physics) 2004 A review of internal transport barrier physics for steady-state operation of tokamaks *Nucl. Fusion* **44** R1
[7] Tala T.J.J., Heikkinen J.A., Parail V.V., Baranov Y.F. and Karttunen S.J. 2001 ITB formation in terms of $\omega_{E\times B}$ flow shear and magnetic shear s on JET *Plasma Phys. Control. Fusion* **43** 507
[8] Liu C.S. 1970 Stabilization of the trapped particle mode by a cool plasma component *Phys. Lett. A* **32** 244–5
[9] Lao L.L. *et al* (the DIII-D Team) 1996 Rotational and magnetic shear stabilization of magnetohydrodynamic modes and turbulence in DIII-D high performance discharges *Phys. Plasmas* **3** 1951–8
[10] Ko S.H., Kim S.S., Jhang H. and Kim J. 2024 Global flux-driven gyrofluid simulations of internal transport barrier formation by external torque in weak magnetic shear configuration *Nucl. Fusion* **64** 086014
[11] Ida K. and Fujita T. 2018 Internal transport barrier in tokamak and helical plasmas *Plasma Phys. Control. Fusion* **60** 033001
[12] Ida K. 2025 Experimental discoveries of a variety of turbulent states of magnetic fusion plasma *Rev. Mod. Plasma Phys.* **9** 8
[13] Taimourzadeh S., Shi L., Lin Z., Nazikian R., Holod I. and Spong D. 2019 Effects of RMP-induced changes of radial electric fields on microturbulence in DIII-D pedestal top *Nucl. Fusion* **59** 046005
[14] Chen Y.C., Qin Y.Q., Sun G.Y. and Lin Z. 2023 The performance of equilibrium radial electric field shear on microturbulence with different magnetic shears in tokamak plasmas *Plasma Phys. Control. Fusion* **65** 075005
[15] Wang W.H., Bao J., Wei X.S., Lin Z., Choi G.J., Dettrick S., Kuley A., Lau C., Liu P.F. and Tajima T. 2021 Effects of equilibrium radial electric field on ion temperature gradient instability in the scrape-off layer of a field-reversed configuration *Plasma Phys. Control. Fusion* **63** 065001
[16] Fu J.Y., Nicolau J.H., Liu P.F., Wei X.S., Xiao Y. and Lin Z. 2021 Global gyrokinetic simulation of neoclassical

ambipolar electric field and its effects on microturbulence in W7-X stellarator *Phys. Plasmas* **28** 062309
[17] Burrell K.H. 1997 Effects of E × B velocity shear and magnetic shear on turbulence and transport in magnetic confinement devices *Phys. Plasmas* **4** 1499–518
[18] Chen Y.C., Qin Y.Q., Sun G.Y., Dong G., Xiao Y. and Lin Z. 2023 Effects of radial electric field on kinetic ballooning mode in toroidal plasma *Phys. Plasmas* **30** 022302
[19] Bao J., Liu D. and Lin Z. 2017 Gyrokinetic ion and drift kinetic electron model for electromagnetic simulation in the toroidal geometry
[20] Abdoul P.A., Dickinson D., Roach C.M. and Wilson H.R. 2015 Using a local gyrokinetic code to study global ion temperature gradient modes in tokamaks *Plasma Phys. Control. Fusion* **57** 065004
[21] Saarelma S., Hill P., Bottino A., Colyer G., Field A.R., McMillan B., Peeters A. and Roach C.M. (the MAST Team) 2012 Global gyrokinetic turbulence simulations of mast plasmas *Plasma Phys. Control. Fusion* **54** 085012
[22] Zhang B. *et al* 2022 Progress on physics understanding of improved confinement with fishbone instability at low q95 textless 3.5 operation regime in east *Nucl. Fusion* **62** 126064
[23] Lin Z., Nishimura Y., Xiao Y., Holod I., Zhang W.L. and Chen L. 2007 Global gyrokinetic particle simulations with kinetic electrons *Plasma Phys. Control. Fusion* **49** B163
[24] Ma Y., Zhang B., Bao J., Lin Z., Zhang W., Cai H. and Li D. 2023 Electrostatic turbulence in east plasmas with internal transport barrier *Nucl. Fusion* **63** 056014
[25] Hahm T.S. and Burrell K.H. 1995 Flow shear induced fluctuation suppression in finite aspect ratio shaped tokamak plasma *Phys. Plasmas* **2** 1648–51
[26] Kishimoto Y., Kim J.-Y., Horton W., Tajima T., LeBrun M.J. and Shirai H. 1999 Toroidal mode structure in weak and reversed magnetic shear plasmas and its role in the internal transport barrier *Plasma Phys. Control. Fusion* **41** A663
[27] Jiang D., Li Y.Y., Wu X.Q., Zhang T., Lyu B., Gao X. and Xu G.S. 2020 Edge toroidal rotation analysis by CXRS diagnostic on east *Fusion Sci. Technol.* **76** 723–30
[28] Xu X., Xu Y., Zhang X. and Hu Y. 2021 Simulations of the radial electric field induced by neutral beam injection in a tokamak *Nucl. Fusion* **61** 086002